

NUMERICAL SIMULATION OF METALLIC SURFACE PLASMA FORMATION BY MEGAGAUSS MAGNETIC FIELDS

Irvin R. Lindemuth, Richard E. Siemon, Bruno S. Bauer, Milena A. Angelova

*University of Nevada, Reno
Reno, Nevada, USA*

Walter L. Atchison

*Los Alamos National Laboratory
Los Alamos, New Mexico, USA*

Sergey F. Garanin

All-Russian Research Institute of Experimental Physics (VNIIEF)

Volodymyr Makhin

*NumerEx, LLC
Albuquerque, New Mexico, USA*

Abstract

Plasma formation on the surface of thick metal in response to a pulsed multi-megagauss magnetic field is being investigated at the University of Nevada, Reno, using aluminum rods that have radii larger than the magnetic skin depth. US and Russian radiation-magnetohydrodynamic codes are being used to help interpret the experimental results such as time of plasma formation and rate of current channel expansion. The best results obtained to date with the UNR code MHRDR use a standard SESAME Maxwell-construct EOS and a Russian resistivity model, and the computed times of formation agree well with the observations across the full range of wire diameters. This leads to the conclusion that plasma formation is an MHD effect and does not involve the non-MHD processes often evoked in other contexts. The computations show that plasma is formed in low-density material that is resistive enough to expand across the magnetic field and yet conductive enough that Ohmic heating exceeds expansion cooling as the expanding material undergoes the liquid-vapor transition.

I. INTRODUCTION

Thick conductors and megagauss magnetic surface fields are encountered in a number of physical situations of current interest: imploding liners, isentropic compression flyer plates, high-current transmission lines, magnetic flux compression generators, and the fuel-pusher interface in Magnetized Target Fusion (MTF). Simple diffusion theory such as given by Knoepfel, Herlach, and others allow a prediction of the surface temperature of solid material as a function of the surface magnetic field, e.g., a temperature of 2 eV would be predicted at 4 MG.

The generation of a low density surface plasma hotter than simple diffusion theory surface temperature estimates has been predicted by Garanin, *et al*[1]. Experiments at the University of Nevada, Reno (UNR), have been designed to test these theoretical predictions and provide a data base for normalizing radiation-magnetohydrodynamic (R-MHD) computer codes.

A. UNR Megagauss Experiment

Plasma formation on the surface of thick metal in response to a pulsed multi-megagauss surface magnetic field is being investigated at UNR with well-characterized experiments [2,3]. Aluminum rods with 0.5-2 mm diameter are pulsed with the UNR Zebra generator (85 kV, 150 kJ, 1 MA, 100 ns). Because the 100-ns, 0.025 eV skin depth of aluminum is approximately 50 μm , the rod radii are larger than the initial magnetic skin depth, in contrast to the much thinner wires typically studied on pulsed power facilities worldwide. The maximum magnetic field at the initial rod radius ranges from 2 MG for the 2-mm-diameter rods to 8 MG for the 0.5-mm-diameter rods.

A number of different load designs have been developed to eliminate end effects, arcing, electric field enhancement, etc. Novel rod mechanical connections and fabrication techniques have resulted in quite uniform visible emission.

Diagnostics include time-resolved imaging, pyrometry, spectroscopy, and laser shadowgraphy. Of particular interest from a computational viewpoint is an array of 16 diodes that image the entire length of the rod. In addition to giving an indication of the uniformity of emission along the rod length, the diode array can be used to determine a surface "brightness temperature" using known geometric, optical, and electrical quantities and an assumption of "black-body" emission. Temperatures so determined reach approximately 30 eV for the thinnest rod.

Report Documentation Page				Form Approved OMB No. 0704-0188	
Public reporting burden for the collection of information is estimated to average 1 hour per response, including the time for reviewing instructions, searching existing data sources, gathering and maintaining the data needed, and completing and reviewing the collection of information. Send comments regarding this burden estimate or any other aspect of this collection of information, including suggestions for reducing this burden, to Washington Headquarters Services, Directorate for Information Operations and Reports, 1215 Jefferson Davis Highway, Suite 1204, Arlington VA 22202-4302. Respondents should be aware that notwithstanding any other provision of law, no person shall be subject to a penalty for failing to comply with a collection of information if it does not display a currently valid OMB control number.					
1. REPORT DATE JUN 2009		2. REPORT TYPE N/A		3. DATES COVERED -	
4. TITLE AND SUBTITLE Numerical Simulation Of Metallic Surface Plasma Formation By Megagauss Magnetic Fields				5a. CONTRACT NUMBER	
				5b. GRANT NUMBER	
				5c. PROGRAM ELEMENT NUMBER	
6. AUTHOR(S)				5d. PROJECT NUMBER	
				5e. TASK NUMBER	
				5f. WORK UNIT NUMBER	
7. PERFORMING ORGANIZATION NAME(S) AND ADDRESS(ES) University of Nevada, Reno Reno, Nevada, USA				8. PERFORMING ORGANIZATION REPORT NUMBER	
9. SPONSORING/MONITORING AGENCY NAME(S) AND ADDRESS(ES)				10. SPONSOR/MONITOR'S ACRONYM(S)	
				11. SPONSOR/MONITOR'S REPORT NUMBER(S)	
12. DISTRIBUTION/AVAILABILITY STATEMENT Approved for public release, distribution unlimited					
13. SUPPLEMENTARY NOTES See also ADM002371. 2013 IEEE Pulsed Power Conference, Digest of Technical Papers 1976-2013, and Abstracts of the 2013 IEEE International Conference on Plasma Science. IEEE International Pulsed Power Conference (19th). Held in San Francisco, CA on 16-21 June 2013.					
14. ABSTRACT Plasma formation on the surface of thick metal in response to a pulsed multi-megagauss magnetic field is being investigated at the University of Nevada, Reno, using aluminum rods that have radii larger than the magnetic skin depth. US and Russian radiationmagnetohydrodynamic codes are being used to help interpret the experimental results such as time of plasma formation and rate of current channel expansion. The best results obtained to date with the UNR code MHRDR use a standard SESAME Maxwell-construct EOS and a Russian resistivity model, and the computed times of formation agree well with the observations across the full range of wire diameters. This leads to the conclusion that plasma formation is an MHD effect and does not involve the non-MHD processes often evoked in other contexts. The computations show that plasma is formed in lowdensity material that is resistive enough to expand across the magnetic field and yet conductive enough that Ohmic heating exceeds expansion cooling as the expanding material undergoes the liquid-vapor transition.					
15. SUBJECT TERMS					
16. SECURITY CLASSIFICATION OF:			17. LIMITATION OF ABSTRACT SAR	18. NUMBER OF PAGES 7	19a. NAME OF RESPONSIBLE PERSON
a. REPORT unclassified	b. ABSTRACT unclassified	c. THIS PAGE unclassified			

The assumption of black-body emission is supported by visible light streaked spectroscopy that shows continuum radiation. Filtered photodiodes observe 16-73 eV photons (VUV) and photons having an energy > 70 eV (EUV) and EUV spectra display emission lines from multiply ionized aluminum, all consistent with the surface brightness temperature.

B. Computational Considerations

The UNR experiments lead to clearly defined, one-dimensional “computer experiments.” The fundamental computational issue is whether or not more-or-less “standard” R-MHD models predict plasma formation under the circumstances of the UNR experiments and whether or not the models accurately predict observables such as the plasma formation time and peak temperature, etc.

In this paper, we report computational results obtained primarily by the UNR Eulerian code MHRDR (Magneto-Hydro-Radiative Dynamics Research). Results from the Los Alamos National Laboratory (LANL) Lagrangian code Raven are also discussed. Results obtained by the Russian UP-MHD Lagrangian code are reported separately by Garanin, *et al.*, in a companion paper in these proceedings [4].

Garanin [1] has elucidated the basic challenges of computationally modeling such experiments. In addition, we note the following issues. As will be shown later, plasma forms near the initial surface and at very low density. This means that Lagrangian codes must expand by a large factor in a very small distance, necessitating very small initial computational cells [4]. Even with small initial cells, a yet-to-be-resolved issue is whether or not Lagrangian computations reach a sufficiently low density, since, in principle, the leading edge of an expansion material may have zero density.

On the other hand, Eulerian codes must have a suitable “vacuum” treatment. Eulerian computational cells can, in principle, make a transition from “vacuum” to “real” material at very low density, although small cells and/or low density may require prohibitively low time steps. Although the Eulerian codes readily admit low density, orders of magnitude change may occur over only a few cells, potentially leading to inaccuracies.

II. COMPUTATIONAL MODEL

The material description used in MHRDR, Raven, and UP-MHD is essentially the same for all codes and is more-or-less standard: a continuity equation, an equation of motion, Faraday’s law, and a material energy equation. Electromagnetic processes are coupled with the Euler equations of hydrodynamics. The equation of motion includes the Lorentz force. Faraday’s law uses a simple Ohm’s law:

$$\vec{E} + \vec{v} \times \vec{B} = \eta \vec{J} = \vec{E}^* \quad (1)$$

where the symbols are, from left to right, the electric field, the material flow velocity, the magnetic field, the electrical resistivity, the electrical current density, and the electric field in the frame of reference of the moving material.

The energy equation includes thermal conduction and Ohmic heating. For completeness, the basic material equations need an equation-of-state (EOS) that gives the specific material energy and pressure as functions of density and temperature. Also needed as functions of density, temperature, and, potentially, magnetic field are the transport coefficients: the thermal conductivity and the electrical resistivity. In the results reported here, the effect of the magnetic field on the transport coefficients is neglected, as justified by Garanin and Kuznetsov [5].

The codes differ somewhat in their treatment of radiation. MHRDR and Raven use a “two-temperature” model whereby a material temperature and radiation temperature are separately computed from the material energy equation and a radiation diffusion equation, respectively. The two equations are coupled through a radiation coupling term. In MHRDR, the coupling term is determined by the Planck opacity and the radiation diffusion is determined by the Rosseland opacity. The radiation equation is “flux limited.”

For the EOS, transport coefficients, and opacities, MHRDR and Raven use SESAME-format computer data base tables. In the computations reported here, we use three different EOS/transport-coefficient combinations as listed in Table 1.

Table 1. EOS/transport-coefficient combinations

Combination Designator	B	C	D
EOS library	SESAME	SESAME	SESVNIF7
EOS table	3719	3719	3710
Resistivity-Conductivity Library	SESAAL	SESVNIF7	SESVNIF7
Resistivity-Conductivity Table	29373	23710	23710

Combination B is a combination that has been widely used to model wires and imploding liners, etc. Combination D is a SESAME-format implementation of analytic models developed at the All-Russian Scientific Research Institute of Experimental Physics (VNIIEF) and is approximately the same as the models described in [4]. As shown in the table, C combines a commonly used SESAME EOS with VNIIEF transport coefficients.

EOS 3719 uses Maxwell constructs, whereas the VNIIEF EOS 3710 has Van-der-Waals loops.

For all combinations, the standard aluminum opacities from the LANL SESOU library are used.

The experimental electric current delivered to the rod provides the magnetic field boundary condition. The current used in all computations reported here is shown in Fig. 1 and is representative of the current actually measured.

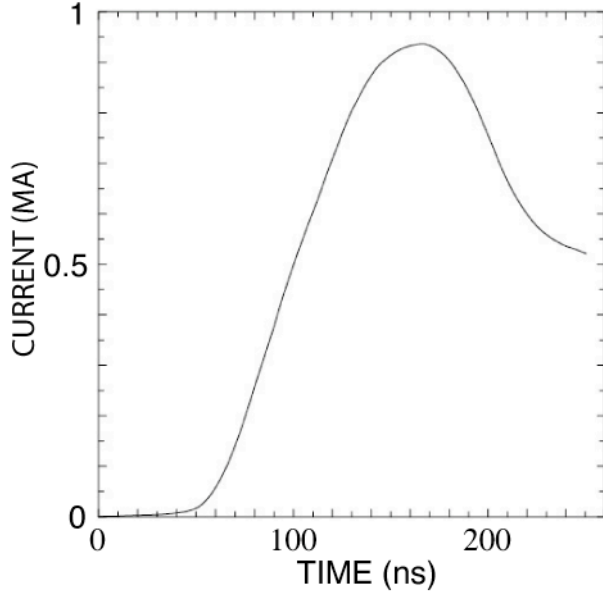


Figure 1. The electrical current used to provide the magnetic field boundary condition in the computations.

Even before turning to the codes, we can gain insight into the physical R-MHD model by examining the characteristic Ohmic heating time. From the Ohmic heating term in the energy equation, we can derive the following equation for the temperature rate of change due to Ohmic heating:

$$\frac{dT}{dt} = \frac{T}{\tau_{oh}} \quad (2)$$

where τ_{oh} is a “characteristic Ohmic heating time” given by

$$\tau_{oh} = \frac{\eta \rho T}{(E^*)^2 (\partial T / \partial \epsilon_m)_\rho} = f(\rho, T, E^*) \quad (3)$$

where ρ is the material density, T is the material temperature, and ϵ_m is the material specific energy.

In Eq. (2), note that τ_{oh} is a function of three quantities, the density, temperature, and electric field in the material frame of reference. Hence, for a fixed value of E^* , we can plot τ_{oh} in the density-temperature plane similar to the way the EOS or transport coefficients are commonly plotted.

Shown in Fig. 2 is τ_{oh} for one EOS-resistivity combination and an electric field characteristic of the Zebra experiments. The τ_{oh} values for other values of the electric field can be determined by scaling the values in Fig. 2 in accordance with Eq. 3.

Under the vapor dome, τ_{oh} is essentially infinite because $(\partial T / \partial \epsilon_m)_\rho$ is zero. Figure 2 shows that at sufficiently low density, τ_{oh} can be sub-nanosecond. We state without showing that, in general, when τ_{oh} is sub-nanosecond, Ohmic heating is dominant over other processes. Hence, plasma can form quickly from vapor at very low (when compared to solid) density and at sufficiently high electric field. There is, however, at each density a minimum temperature below which plasma cannot form in the time-scale of the experiment.

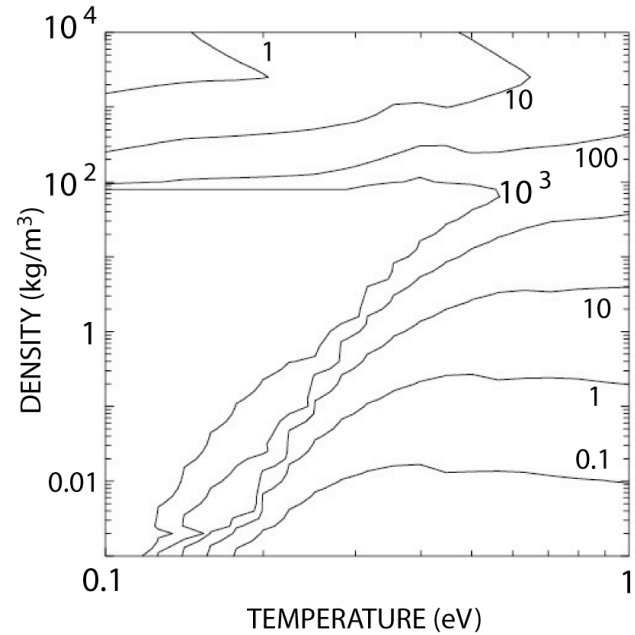


Figure 2. The characteristic Ohmic heating time τ_{oh} (ns) for EOS/transport combination C for $E^* = 2$ MV/m, a typical value for the Zebra experiments.

In accordance with Eq. 2, τ_{oh} is an “e-folding time.” If Ohmic heating is dominant and τ_{oh} is constant, the temperature will increase exponentially. However, as shown in Fig. 2, in some parts of the density-temperature plane, τ_{oh} can change by several orders of magnitude when the temperature changes by only a small fraction because of the rapid decrease in electrical resistivity with increasing temperature. Thus, the temperature can rise even faster than exponentially.

Combinations B and D have similar behavior to that shown in Fig. 2, although the places in the density-temperature plane where τ_{oh} changes rapidly differ slightly, and these differences lead to significant differences in the computed results.

III. COMPUTED RESULTS

Shown in Figures 3-6 are the experimental surface brightness temperatures for four rod sizes for which plasma formation is observed and the corresponding MHRDR computational results. The MHRDR value plotted is the radiation temperature at the real/vacuum interface. In both the experiments and the computations, the plasma formation occurs at a later time and the peak brightness temperature decreases as the rod diameter is increased.

Combinations C and D agree reasonably well with the observed plasma formation time and peak temperature, although the computed rate of rise of temperature is somewhat greater than in the experiment. On the other hand, combination B shows plasma formation later than observed and a lower peak temperature. In addition, combination B does not show plasma formation at a diameter of 1.25 mm.

Even though the radiation models different, the MHRDR results using combination D are in good agreement with the UP-MHD results [4].

In the MHRDR computations, plasma forms at a density near the “cutoff density” value which is used to distinguish cells which contain “real” material and cells which contain “vacuum.” For the computations reported in this paper, the cutoff density value is 0.001 kg/m^3 .

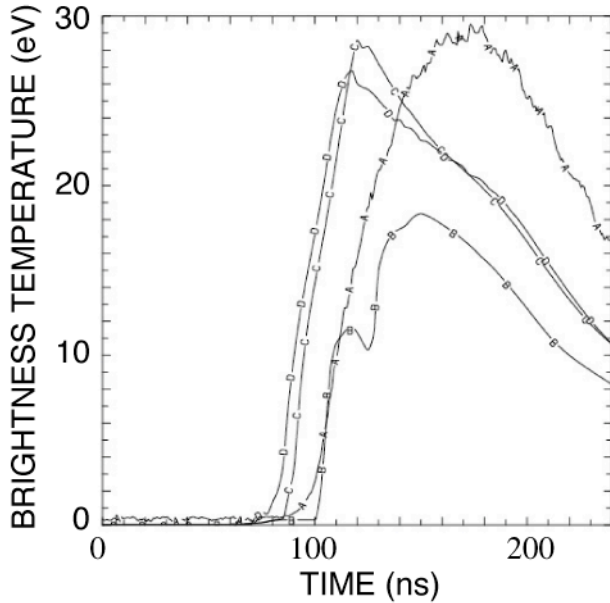


Figure 3. The experimental (A) and computed (B, C, D) surface brightness temperature for a 0.5-mm-diameter rod: (B) EOS/transport combination B; (C) EOS/transport combination C; (D) EOS/transport combination D.

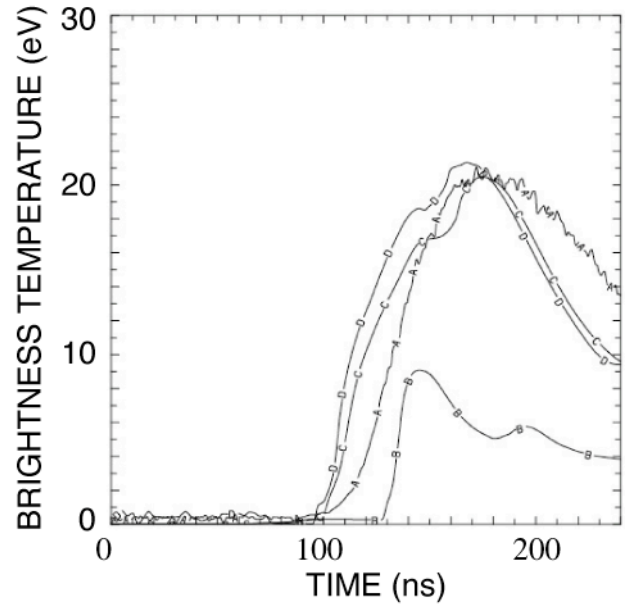


Figure 4. The experimental (A) and computed (B, C, D) surface brightness temperature for a 0.8-mm-diameter rod: (B) EOS/transport combination B; (C) EOS/transport combination C; (D) EOS/transport combination D.

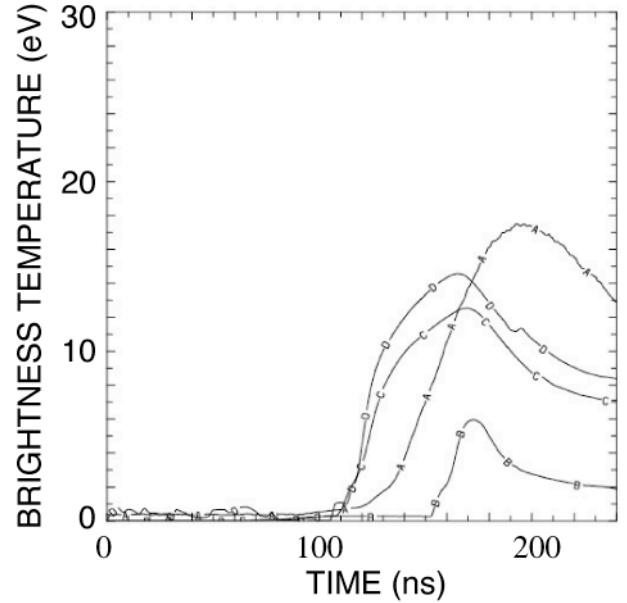


Figure 5. The experimental (A) and computed (B, C, D) surface brightness temperature for a 1-mm-diameter rod: (B) EOS/transport combination B; (C) EOS/transport combination C; (D) EOS/transport combination D.

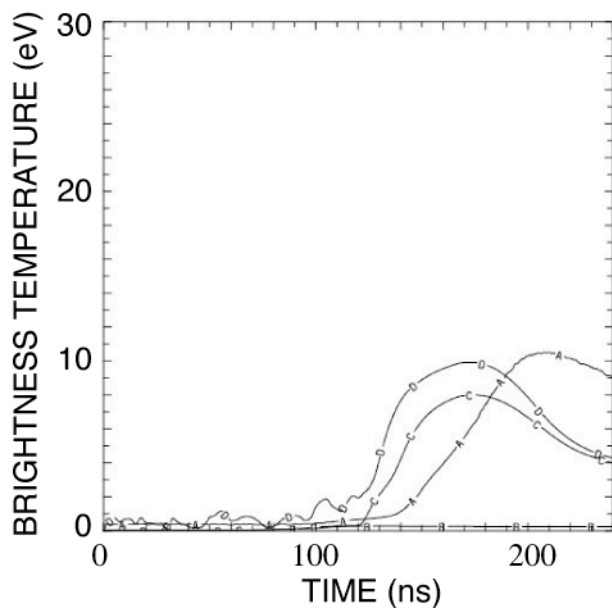


Figure 6. The experimental (A) and computed (B, C, D) surface brightness temperature for a 1.25-mm-diameter rod: (B) EOS/transport combination B; (C) EOS/transport combination C; (D) EOS/transport combination D.

Shown in Figures 7-9 are radial profiles of key quantities in the initial plasma formation process. At earlier times, the temperature profile (Fig. 8) decreases to zero essentially linearly, and the slight “bump” in temperature at the leading edge is not present. Plasma forms when material enters the low τ_{oh} region (Fig. 9). As shown in Fig. 8, this occurs when the temperature at the leading edge reaches approximately 0.2 eV. Fig. 7, curve C, shows that once plasma forms, the magnetic field temporarily stops the expanding material.

Eq. 2 provides a means of checking the computational results. The electric field at the material boundary can be determined by looking at the rate of change of flux within the material because plasma formation takes place before the magnetic diffusion wave reaches the axis. Because the electric field so determined is based upon an integral quantity, it is not as likely to have numerical inaccuracies as one determined based upon local quantities at the plasma boundary, since the latter is potentially subject due to large errors because of the large resistivities involved. Because the plasma formation takes place rapidly, it takes place at approximately constant density and electric field. Therefore, choosing a temperature near but before plasma formation in the computations as an initial value for Eq. 2, Eq. 2 can be integrated. If the computations are correct, the result of integrating Eq. 2 should be very close to the temperature rise in the computations. When we have performed such a check, the solution to Eq. 2 and the computations agree satisfactorily.

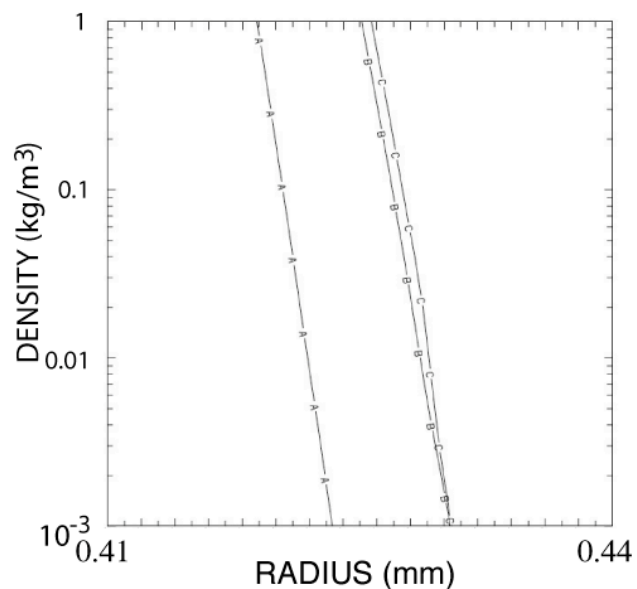


Figure 7. The computed density in the leading edge of the expanding material for a 0.8-mm-diameter rod at (A) 97.5 ns; (B) 99.8 ns; (C) 100 ns. Note the expanded radial scale. EOS/transport combination C is used.

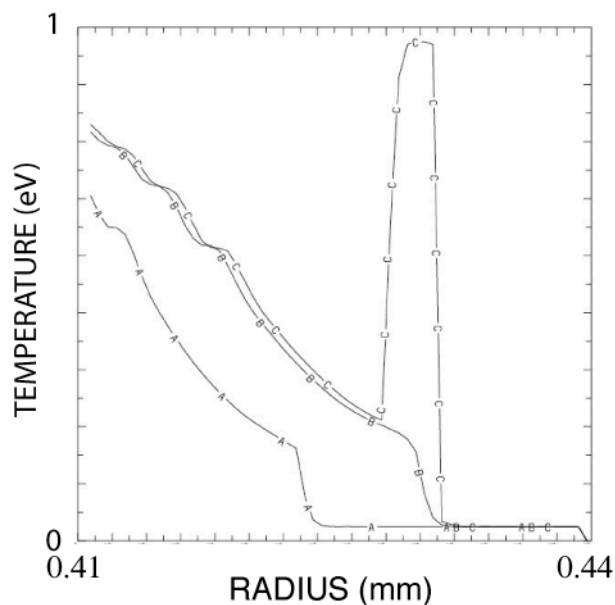


Figure 8. The computed temperature in the leading edge of the expanding material for a 0.8-mm-diameter rod at (A) 97.5 ns; (B) 99.8 ns; (C) 100 ns. Note the expanded radial scale. EOS/transport combination C is used.

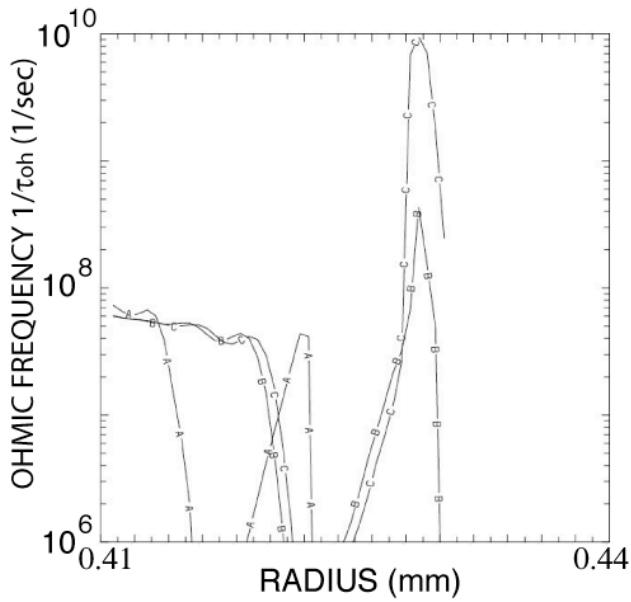


Figure 9. The computed inverse of the characteristic Ohmic heating time, τ_{oh} , in the leading edge of the expanding material for a 0.8-mm-diameter rod at (A) 97.5 ns; (B) 99.8 ns; (C) 100 ns. Note the expanded radial scale. EOS/transport combination C is used.

Although we have not compared Raven and MHRDR results for all rod radii and all EOS/transport combinations, we have found that the two codes show satisfactory agreement. Because Raven is a Lagrangian code, studying the processes that occur to any piece of the material is relatively easy, since each Lagrangian cell tracks a specific piece of material, in contrast to the Eulerian code MHRDR where material flows into or out of each cell.

Raven using combination B shows plasma formation in its outermost cell. For the outer cell, because the resistivity of the cell becomes very high as the material melts, the Lorentz force is much smaller than the pressure gradient force, so, with regard to momentum, the expansion into vacuum of this material is essentially a “free expansion.” On the other hand, Raven shows a perhaps surprising result. Even though the resistivity of the material is high, the electric field is high enough that Ohmic heating exceeds the expansion cooling. Therefore, the expansion process is non-adiabatic, and energy is deposited in the material as it expands and traverses the vapor dome.

The experiment and computations suggest that there is a magnetic field threshold for plasma formation. Shown in Table II are approximate values at plasma formation. The maximum computed brightness temperature for the 1.6-mm-diameter rod is about 3 eV.

The maximum magnetic field reached at 2-mm-diameter, where plasma does not form either experimentally or computationally, is 2 MG, which is

below the computational threshold of approximately 2.4 MG. Garanin [1] predicted a 3 MG threshold for copper.

Table II. Approximate values when computed brightness temperature reaches 1 eV (combination C).

Rod diameter	Time (ns)	Magnetic Field (MG)	Electric Field (MV/m)
0.5	86.9	2.45	2.54
0.64	92.5	2.48	2.45
0.8	102.6	2.43	1.91
1	113.4	2.37	1.55
1.25	127.5	2.34	1.49
1.6	151.0	2.15	0.85

We summarize briefly some other computational results using MHRDR and combination C. The surface plasma forms before the inward shock and magnetic diffusion wave reaches the axis. Once the inward shock reaches the axis, Ohmic heating maintains the core temperature as the core expands. The thinnest wire (0.5-mm-diameter) takes on a “thin” wire characteristic where most of the current is carried by a low-density corona. For the larger wires, e.g., 1-mm-diameter, the corona carries a small fraction of the current. Thermal conduction and radiation limit the peak surface temperature but do not affect the time of plasma formation temperature. Because the plasma layer is not optically thick, the “observed” brightness temperature is lower than the peak temperature in the layer. The MHRDR results are reasonably converged with respect to “cutoff density” and radial cell size (the cell size for the computations reported here is 0.5 μm). If the “cutoff density” is too high (e.g., 1 kg/m^3 at 1.25-mm-diameter), plasma will not form in the computations.

IV. CONCLUDING REMARKS

With the appropriate EOS-transport combination, MHRDR accurately predicts experimental observables such as time of plasma formation, brightness temperature, and radial expansion, and trends in the observables as the rod radius is varied. With observables and trends accurately predicted, it seems reasonable to conclude that plasma formation in the Zebra experiments is a “thermal” process driven by Ohmic heating. Analogous plasma formation must be considered a possibility and accurately modeled in other “thick” conductors subjected to megagauss magnetic fields.

There are some remaining computational and experimental issues. Is the plasma formation process different when an EOS that has Van-der-Waals loops is used compared to when an EOS with Maxwell constructs is used? Why is there a magnetic field threshold and what determines it? What processes (e.g., shocks, Ohmic heating) are involved as the rod progresses from a small amount of optically thin, low-density, extremely low mass

initial surface plasma to a radiating plasma visible on the diagnostics? How important are two-dimensional effects (late time shadowgrams show some instability growth)? What is the role, or lack thereof, of other mechanisms, e.g., photoionization?

It is anticipated that the computational and experimental results will be refined. Effects of some experimental variation in the peak current will be explored computationally. Experimental reproducibility will be evaluated and some timing discrepancies will be resolved.

Finally, the experimental and computational techniques should be extended to different materials of interest, e.g., tungsten. Because the EOS and transport properties of other materials are not as well understood as aluminum, it may be more difficult to obtain the agreement between experiment and computation reported here.

The authors would like to acknowledge the excellent experimental work conducted by our UNR colleagues Thomas Awe and Dr. Stephan Fuelling.

V. REFERENCES

- [1] S. F. Garanin, G. G. Ivanova, D. V. Karmishin, and V. N. Sofronov, "Diffusion of a megagauss field into a metal," *J. Appl. Mech. Tech. Phys.*, vol. 46, pp. 153-159, 2005.
- [2] T. J. Awe, B. S. Bauer, R. E. Siemon, *et al.*, "Plasma formation and evolution from thick aluminum wires pulsed with megagauss field," presented at XII Int. Conf. on Megagauss Magnetic Field Generation and Related Topics, Novosibirsk, Russia, 2008.
- [3] S. Fuelling, T. J. Awe, B. S. Bauer, *et al.*, "A Zebra experiment to study plasma formation by megagauss fields," *IEEE Trans. Plasma Sci.* vol. 36, pp. 62-69, 2008.
- [4] S. F. Garanin, S. D. Kuznetsov, W. L. Atchison, *et al.*, "Numerical Simulations of Thick Aluminum Wire Behavior Under Megaampere Current Drive," these Proceedings.
- [5] S. F. Garanin and S. D. Kuznetsov, "The Role of Electron Heat Conductivity and Radiation Transport in 1D Simulation of Wire Explosions in Zebra Experiments," these Proceedings.